PCCP

Accepted Manuscript

ROYAL SOCIETY OF CHEMISTRY

www.rsc.org/pccp

Ga-doped TiZnO Transparent Conductive Oxide used as an alternative anode in blue, green, and red phosphorescent OLEDs

Chih-Hao Chang,* Wei-Sheng Liu,* Shen-Yu Wu, Jun-Lin Huang, Chao-Yu Hung, Yu-Lin Chang, Ying-Chieh Wu, Wei-Chih Chen and Yi-Cheng Wu

Department of Photonics Engineering, Yuan Ze University, Chung-Li, Taiwan 32003

E-mail: chc@saturn.yzu.edu.tw; Fax: + 886 3 4638800 ext. 7517; Tel: + 886 3 4514281

E-mail: wsliu@saturn.yzu.edu.tw; Fax: + 886 3 4638800 ext. 7521; Tel: + 886 3 4514281

Abstract

X-ray diffraction was used to study the optoelectronic characteristics of Ga-doped TiZnO (GTZO) thin film and revealed increased crystallinity with annealing temperatures ranging from as-grown to 450 °C. The low thin film resistivity of 6.1×10^{-4} Ω-cm and the average high optical transmittance of 93% in the wavelength range between 350 and 800 nm makes GTZO an alternative candidate for application in organic light-emitting diodes (OLEDs). Both GTZO and indium-tin-oxide (ITO) anodes are employed for the successful fabrication of blue, green, and red phosphorescent OLEDs. The similar device electrical characteristics observed could be interpreted as evidence of the effectiveness of doping Ga in TiZnO. The simplified tri-layer blue, green, and red phosphorescent OLEDs demonstrated high performance with respective maximum efficiencies of 19.0%, 14.5%, and 9.1%, representing an improvement over ITO-based OLEDs. Furthermore, the OLEDs with the GTZO anode exhibited superior performance at higher current densities, demonstrating high potential for employment in OLED displays and lighting applications.

Introduction

Increasing attention is being devoted to fundamental and applied research in organic light-emitting diodes (OLEDs) due to their potential applications in displays and solid-state lighting. However, the surge of human-machine interfaces in a variety of electronic applications has raised demand for indium-tin-oxide (ITO), which may likely lead to indium shortages. In addition, ITO itself suffers from a number of disadvantages: it is chemically instable, potentially harmful to humans and unsuitable for use with flexible substrates. Consequently, new research efforts have focused on the development of alternative indium-free transparent conducting oxides (TCOs), which have been shown to have characteristics comparable to ITO, including low sheet resistance, high optical transmittance, wide band gap, adequate work function and low cost fabrication.

Among these substituents, zinc oxide (ZnO) thin films are seen as being among the most promising because of their low material cost, high chemical stability, ease of doping, non-toxicity, and optoelectronic properties which are equal to or potentially superior to those of typical ITO films.[1-5] The electrical resistivity of a ZnO thin film can be further improved by impurity doping of Group III elements such as B^{3+} , Ga^{3+}, and Al^{3+} to replace Zn^{2+} ions in a ZnO crystal lattice to provide an extra electron.[6-8] Among these candidates, Ga-doped ZnO (GZO) has been studied extensively, and is considered to be the most promising TCO material because its enhanced optoelectronic properties are comparable to those found in ITO.[9-10] Moreover, GZO thin films with close Ga-O and Zn-O bond lengths of 1.92 Å and 1.97 Å, respectively, exhibit reduced crystal defects resulting from lattice strain, and high electrochemical stability. The advantages of the proposed crystal lattice length result in highly reliable GZO based optoelectronic devices. In addition, the smooth GZO surface contributed by the surfactant effect of Ga doping in ZnO is beneficial for the development of various optoelectronic devices, particularly OLED applications.[8,10]

Compared to ITO used in OLEDs, GZO anodes have a slightly better sheet resistance and

transparency in the visible spectral region. In 2008, J. J. Berry *et al.* reported green fluorescent OLEDs using GZO anodes have operating voltages and external quantum efficiencies slightly lower than those obtained by devices fabricated with similar architecture by using commercial ITO anodes.[11] On the other hand, aluminum-doped ZnO (AZO) is also an inexpensive nontoxic material with electrical and optical properties comparable to those of ITO. In 2008, J. Meye *et al.* demonstrated green phosphorescent OLEDs (PhOLEDs) produced with AZO anodes.[12] At a practical luminance of 100 cd/m^2, they achieved power and luminance efficiencies up to 27 lm/W and 44 cd/A, respectively, while the turn on voltage (V_{on}) was only 4.0 V. Another example was reported by H.-H. Park in 2013, using red PhOLEDs to probe the capability of the AZO anode.[13] OLED performance was found to benefit from the anode's sheet resistance and high transmittance. However, the low work function of 4.2 eV might block the hole injection and thus leading to a higher turn on voltage of 5.3 V. In 2012, J.-J. Kim's group proposed a new transparent electrode constructed by mixing TiO_2 and ITO.[14] This TITO film possesses a low sheet resistance of 18.06 Ω/sq and a good average transmittance of 86.33%. Furthermore, the work function (4.71 eV) of TITO could smooth the carrier injection into the organic layer. Green PhOLEDs based on the TITO anode demonstrated high efficiencies of 21.69% (90.92 lm/W) and a low turn-on voltage of 4.0 V.

Compared with the Group III elements, TiO_2 doped ZnO (TZO) exhibits Ti^{4+} (ionic radius: 0.68 Å) substitution for Zn^{2+} (ionic radius: 0.72 Å) ions and hence behave as a donor providing an extra two free electrons, thus increasing thin-film conductivity.[15] Although the Ti atoms may incorporate interstitially into the ZnO hexagonal crystal lattices, a moderate concentration of Ti atoms not only reduces the number of Ti^{4+} carrier scattering centers, but also increases the grain size of the TZO thin film and increases the optical transmittance.[16] Therefore, in this study, we propose to combine the advantages of Ga and Ti elemental doping in ZnO as a high performance Ga-doped TiZnO (GTZO) for OLED applications. More importantly, the film fabrication does not require expensive equipment for atomic layer deposition (ALD) or

metal-organic chemical vapor deposition (MOCVD). This high quality GTZO film could be obtained simply by using the relatively inexpensive radio-frequency (RF) magnetron sputtering technique.

Experimental

Preparation of TCO films. The Ga-doped TiZnO films were grown using a 3 in. $ZnO/Ga_2O_3/TiO_2$ (96/3/1wt.%, purity 99.99%) target. All GTZO films were deposited at room temperature (RT) by RF magnetron sputtering on glass substrates. Prior to deposition, the targets were pre-sputtered for 3 min. The sputtering chamber was evacuated with a high-vacuum pressure of approximately 4×10^{-6} Torr, and a working pressure of 5.0×10^{-3} Torr was maintained with an argon (Ar) gas flow of 30 standard cubic centimeters per min (sccm). The RF sputtering power was kept at 150 W. During deposition, the chamber was cooled using a water-cooled chiller system, and the thickness of the deposited GTZO film was maintained at 300 nm to obtain preferable TCO properties with high conductivity and transparence.[5,17] The GTZO samples were then thermally post-annealed for 3 min in nitrogen ambient at temperatures ranging from 150 to 550 °C in a rapid thermal annealing (RTA) system.

Electrical and Photophysical measurement. Electrical resistivity, mobility, and carrier concentration were measured by a Hall measurement system using the van der Pauw configuration at RT. XRD with a copper $K\alpha_1$ (λ = 1.54052 Å) source was used to characterize the crystalline structure of the thin films. Optical transmission measurements were conducted with a UV/VIS spectrophotometer (Shimadzu UV-1650PC).

OLED Fabrication. GTZO and ITO films were selected as the transparent anode material for OLED fabrication. The organic materials for the small molecules used were purchased from Nichem and Lumtec. All organic compounds were subjected to temperature-gradient

sublimation under high vacuum before use. The organic and metal layers were deposited by vacuum evaporation in a vacuum chamber with a base pressure of $<10^{-6}$ Torr. The deposition system enabled the fabrication of the complete device structure without breaking the vacuum. Current-voltage-luminance (*I-V-L*) characterization of the devices was performed using an Agilent 4156C semiconductor parameter analyzer and a Si photodiode calibrated with a Photo Research PR650. Electroluminescence spectra of the devices were recorded using an Ocean Optics spectrometer.

Results and Discussion

Figure 1 (a) presents the crystalline structure and orientation of the GTZO films investigated by X-ray diffraction (XRD). The diffractogram angles of the thin films show that all the XRD patterns exhibit a prominent (002) peak for the deposited films with annealing temperatures ranging from as-grown to 450°C. The XRD peak intensity increases with annealing temperature, i.e. the crystal quality of the GTZO thin film improves at high annealing temperatures. Figure 1 (b) depicts the full width at half-maximum (FWHM) and 2θ value of (0 0 2) peak position of films annealed at different temperatures. The (0 0 2) peak position of the GTZO films represents values from 32.24° to 34.40°, which is smaller than the corresponding value of bulk ZnO material (34.42°) and implies the presence of compressive strain in the thin film because of the incorporation of Ti atoms in the ZnO crystal.[18] The FWHM significantly decreases from 0.44° to 0.39° for annealing temperatures ranging from RT to 450°C. However, the decrease in XRD (002) peak intensity and the broadened FWHM were observed as the annealing temperature increased to 550 ^{o}C. This high-temperature annealing process was considered to result in the decomposition or desorption of Zn and O atoms from the GTZO films, thereby deteriorating the crystallinity.[19-20] The narrow FWHM indicates increased average crystallite size via Schereer's theorem calculation. Therefore, the formation of larger crystallites at 450°C is responsible for the improved crystal intensity in the XRD study because

of high-thermal energy contributing to the coalescence of adjacent grains.[21-22] GTZO TCO thin films with large crystallite size can reduce the grain-boundary scattering and increase the Hall carrier mobility, thus contributing to the increased thin-film conductivity.[23]

Figure 2 shows an average high transmittance of 93 % in the wavelength region of 350-800 nm, and a sharper transmission band edge than that of the ITO thin film in the inset. The high transmittance of GTZO films in this work indicates superior optical properties compared to those of typical ITO thin films.[24-25] The optical band gap (E_g) of the GTZO films was calculated by considering an electron transition from valence to the conduction band when the thin film absorbs a photon of energy ($h\nu$). In a semiconductor with a direct band gap, the absorption coefficient (α) obeys the following relationship for E_g:[26]

$$(\alpha h\nu)^2 = (h\nu - E_g) \qquad (1)$$

where h is the Planck constant, and ν is the photon frequency. The optical band gap (E_g) is therefore deduced by extrapolating the linear portion of a plot $(\alpha h\nu)^2$ against the ($h\nu$) axis.

The direct optical band gaps of GTZO films with different annealing temperatures were evaluated from the Tauc plot (Figure 3). The results show an increased optical band gap from 3.54 to 3.58 eV as the annealing temperature increased from RT to 450^{o}C, which is mainly attributed to the Burstein–Moss effect, i.e., shifts of the Fermi level due to increased electron concentration.[27-28] This postulated carrier increment agrees well with the Hall measurement results. Figure 4 shows the electrical resistivity (ρ), mobility (μ), and carrier concentration (n) of the GTZO films as a function of the post-annealing temperature. The resistivity of the GTZO films decreased from 1.15×10^{-3} to 6.10×10^{-4} Ω-cm as annealing temperatures increased from 150 to 450°C. The GTZO thin film produces its lowest resistivity at an annealing temperature of 450 °C, with a carrier concentration of 4.10×10^{21} cm^{-3} and mobility of 7.66 cm^2/Vs. The increased carrier concentration of the GTZO thin film (>10^{21} cm^{-3}) over that of typical GZO thin films can be attributed to the contribution by Ti doping. We also employed sputtering to deposit an ITO film with a thickness of 300 nm. GTZO and ITO films with same thickness were compared to further examine the fabricated TCO films used in the OLEDs. Table I

summarizes the electrical and optical properties of GTZO (annealed at 450℃) and the fabricated ITO films. Compared to the GTZO film, the fabricated ITO film exhibits a lower carrier concentration of 8.48×10^{20} cm^{-3} and a higher mobility of 22.4 cm^2/Vs. Furthermore, the ITO film exhibited a sheet resistance of 10.9 Ω/sq, as opposed to 20.3 Ω/sq for the GTZO film. On the other hand, as shown in Fig. 1, the transmittance of the ITO film was much lower than that of GTZO film. A 300 nm-thick GTZO film was used to produce a low sheet resistance while an ITO film of identical thickness resulted in inferior transmittance. To evaluate the performance of GTZO and ITO TCO, this study employed the figure of merit (Φ_{TC}), expressed as $\Phi_{TC} = T^{10}/R_S$, where T is the average transmittance in a visible wavelength region (350 – 800 nm), and R_S is the sheet resistance of the TCO structure. The Φ_{TC} is the calculated result of GTZO and ITO thin films and is shown in Table I to be 23.84 and 12.61×10^{-3} Ω^{-1} for the GTZO and ITO thin films, respectively.

Table I. Electrical and optical properties, and Figure of merit for the GTZO and ITO films.

	Figure of merit Φ_{TC} ($\times10^{-3}$ Ω^{-1})	**Transmittance** (%) [350 – 800 nm]	**Resistivity** (Ω-cm)	**Sheet resistance** (Ω/sq)	**Carrier concentration** (cm^{-3})	**Mobility** (cm^2/Vs)	**Work function** (eV)
GTZO	23.84	85% ~100%	6.10×10^{-4}	20.3	4.10×10^{21}	7.66	4.84
ITO	12.61	75% ~90%	3.27×10^{-4}	10.9	8.48×10^{20}	22.4	4.75

Encouraged by aforementioned results, we tried to design PhOLEDs using both GTZO and ITO as anodes. Processes such as charge injection, balanced charge transport and exciton confinement within the emissive layer have to be optimized to produce good output from the light emitting device. The tested devices were developed using the well-known blue, green, and red iridium complexes FIrpic, *fac*-$Ir(ppy)_3$ and $Ir(piq)_2$acac. Furthermore, the host material 3-bis(9-carbazolyl)benzene (mCP) was chosen as the emitting host due to its wide energy gap and bipolar transport capability, allowing for the convenient adjustment of the carrier recombination location and the carrier balance.[29-30] In addition, the device was completed using the wide triplet-gap materials di-[4-(N,N-ditolyl-amino)-phenyl] cyclohexane (TAPC) and

1,3,5-tri[(3-pyridyl)-phen-3-yl]benzene (TmPyPB), respectively, as the hole-transport layer (HTL) and electron-transport layer (ETL).[31-34] The respective hole and electron mobilities of TAPC and TmPyPB are about 10^{-2} and 10^{-3} cm^2/Vs, and possess wide triplet gaps (E_T) of about 2.87 and 2.78 eV, respectively, facilitating high energy exciton confinement. Therefore, we constructed the PhOLEDs with a simplified architecture using GTZO (Device 1) or ITO (Device 2) (300 nm)/TAPC (35 nm)/ mCP doped with 8.0 wt.% Emitter (25 nm)/ TmPyPB (40 nm)/LiF (0.8 nm)/Al (150 nm), with aluminum used as the cathode. The structural drawing of the materials and schematic structures of the tested blue PhOLEDs are shown in Fig. 5.

The corresponding electroluminescence (EL) characteristics are shown in Fig. 6 and Table II. From Fig. 4(a), considering the different inherent photophysical properties of GTZO and ITO films, the spectral differences detected between them could be likely attributed to the different effects of optical interference. By comparing the EL spectra of Devices B1 and B2, the GTZO-based OLED exhibited a stronger intensity ranging from 500 to 550 nm, which benefits the color rendering capability of white OLEDs. On the other hand, the emission of both devices was stable within a wide luminance range from 10^2 to 10^4 cd/m^2, indicating that the carrier recombination was confined within the emitting layer and that exciton diffusion to the adjacent layers was avoided. The corresponding CIE coordinates of Devices B1 (GTZO) and B2 (ITO) at a practical luminance of 10^3 cd/m^2 are (0.16, 0.32) and (0.17, 0.37). The current density-voltage (*J-V*) and luminance-voltage (*L-V*) curves of tested devices are shown in Figs. 4(b) and 4(c). Although Devices B1 and B2 exhibited similar current density-voltage curves, improved luminance could be obtained through employing the GTZO film as the OLED anode. The respective turn-on voltages for Devices B1 and B2 defined at a luminance of 1 cd/m^2 were the same at 3.3 V. The identical turn-on voltage of both devices is mainly attributed to their similar work functions. In addition, Device B1 achieved a maximum luminance of 40573 cd/m^2 at 12.8 V, while Device B2 had a peak luminance of 59287 cd/m^2 at an operating voltage of 10.6 V. The higher driving voltage and luminance recorded implied that OLEDs with GTZO

anodes could sustain a stronger electrical field.

From the efficiency curves shown in 4(d) and Table II, Device B1 exhibited peak EL efficiencies of up to 19.0 %, 40.9 cd/A, and 42.4 lm/W. Similarly, based on the same device architecture, Device B2 exhibited maximum efficiencies of 18.4 %, 40.1 cd/A, and 41.9 lm/W. In addition, Device B1 exhibited EL efficiencies of 16.2%, 34.8 cd/A and 25.3 lm/W at a practical brightness of 10^2 cd/m^2; while Device B2 exhibited efficiencies of 15.8%, 34.5 cd/A and 25.6 lm/W. The superior efficiencies obtained in Device B1 confirmed that the carrier balance could be easily adjusted. In common PhOLEDs, triplet-triplet annihilation (TTA) is seen as being responsible for significant decreases in efficiency in higher luminance regimes. The external quantum efficiency of the here reported PhOLEDs declined by half at a current density ($J_{1/2}$) of 92 and 98 mA/cm^2, respectively, for Devices B1 and B2.[35-36] The similar efficiency roll-off behaviors and *J-V* curves indicate that the exciton formation zone was similarly located for both devices during the operation. Hence, we can deduce that the spectral difference between both devices is certainly caused by the optical influence.

Table II. EL characteristics of tested devices with different anodes.

Device		**B1**	**B2**	**G1**	**G2**	**R1**	**R2**
Emitter		FIrpic		*fac*-Ir(ppy)$_3$		Ir(piq)$_2$acac	
Electrode		GTZO	ITO	GTZO	ITO	GTZO	ITO
External Quantum Efficiency (*EQE*) (%)	[a]	19.0	18.4	14.5	13.5	9.1	7.4
	[b]	16.2	15.8	14.5	13.4	5.5	4.4
Luminance Efficiency (*LE*) (cd/A)	[a]	40.9	40.1	50.0	48.5	6.6	5.4
	[b]	34.8	34.5	49.9	48.1	2.2	1.7
Power Efficiency (*PE*) (lm/W)	[a]	42.4	41.9	50.4	44.9	6.3	5.1
	[b]	25.3	25.6	42.9	39.8	3.8	3.1
V_{on} (V)	[c]	3.3	3.3	3.1	3.1	3.3	3.4
$J_{1/2}$ (mA/cm^2)		92	98	119	115	8	11
Max. Luminance (cd/m^2) [Voltage]		40573 [12.8 V]	59287 [10.6 V]	62897 [13.0 V]	52597 [10.2 V]	8192 [14.2 V]	7170 [12.0 V]

CIE1931 coordinates	[b]	(0.16, 0.32)	(0.17, 0.37)	(0.34, 0.60)	(0.33, 0.62)	(0.68, 0.31)	(0.68, 0.32)
	[d]	(0.16, 0.32)	(0.16, 0.36)	(0.34, 0.60)	(0.33, 0.62)	(0.68, 0.31)	(0.68, 0.32)

[a] Maximum efficiency; [b] recorded at 10^2 cd/m^2; [c] turn-on voltage measured at 1 cd/m^2; [d] measured at 10^3 cd/m^2.

As mentioned in the discussion for blue OLEDs above, similar EL characteristics and slightly superior performance of green and red PhOLEDs with different transparent anodes were observed. For instance, the respective maximum efficiencies of Devices G1 and G2 were 14.5% and 13.5%, while those of Devices R1 and R2 were 9.1% and 7.4%. The similar turn-on voltages and current densities observed in each devices are owing to the similar work functions of both anodes with the UV-Ozone treatment. Furthermore, in spite of the phosphors possessing different energy bandgaps, carrier balance could be realized in all GTZO-based devices with a simplified tri-layer architecture. Overall, comparing the efficiencies of the tested blue, green, and red PhOLEDs indicate that the EL characteristics of devices based on different anodes are comparable. Moreover, in Table III, we collect the EL characteristics of OLEDs with different anodes from selected articles published during 2003~2014.[13-14, 37-43] The performance of the GTZO-based OLEDs were not inferior to those of other previously-reported TCO candidates. This outstanding performance manifests the great potential of GTZO films as an alternative anode for OLEDs.

Table III. The EL characteristics of OLEDs with different anodes from selected articles.

Year	TCO	Emitter (*emission color*)	*EQE* (%) [a]	*LE* (cd/A) [a]	V_{on} (V) [b]	Author [ref.]
2003	ZZO (Zr:ZnO)	Alq_3 (green)	0.87	—	~ 3.0	H. Kim *et al*. [37]
2007	AZO (Al:ZnO)	*fac*-Ir(ppy)$_3$ (green)	—	54.6	< 2.8	Y. Tomita *et al*. [38]
2008	AIZO (Al:In:ZnO)	Alq_3 (green)	—	—	~ 3.0	J. H. Bae *et al*. [39]
2008	IZO (In:ZnO)	*fac*-Ir(ppy)$_3$ (green)	13.2	—	~ 3.7	J. W. Kang *et al*. [40]
2010	GZO (Ga:ZnO)	FIrpic (blue)	15.2	—	~ 4.1	L. Wang *et al*. [41]
2010	ZnO NPs	FIrpic (blue)	8.2	16.5	~ 7.0	H. Lee *et al*. [42]

2011	TZO (Ti:ZnO)	Alq_3 (green)	—	~ 2.3	~ 3.0	Z. L. Tseng *et al*. [43]
2012	TITO (Ti:ITO)	*fac*-Ir(ppy)$_3$ (green)	21.7	—	< 3.0	J. W. Lim *et al*. [14]
2013	AZO (Al:ZnO)	RP-411 (red)	—	5.4	~ 4.6	S. C. Gong *et al*. [13]
2014	GTZO	Ir(piq)$_2$acac (red)	9.1	6.6	3.3	This work
		fac-Ir(ppy)$_3$ (green)	14.5	50.0	3.1	
		FIrpic (blue)	19.0	40.9	3.3	

[a] Maximum efficiency; [b] turn-on voltage measured at 1 cd/m^2.

In summary, we have investigated the development of high-quality GTZO films by radio-frequency magnetron sputtering combined with a rapid thermal annealing process. Experimental results show that the annealing process improves the structural, electrical and optical properties of GTZO films, resulting in improved resistivity, electron mobility and carrier concentrations of 6.1×10^{-4} Ω-cm, 7.66 cm^2/Vs and 4.1×10^{21} cm^{-3}, respectively. High average optical transmittance of 93 % at wavelengths of 350-800 nm was achieved in GTZO TCO through annealing at 450 °C. These superior TCO characteristics further verify the suitability of high quality GTZO thin film for OLED applications. The exhibited electrical and optical capabilities provide room for adjusting the carrier balance and emission colors of OLEDs. Thus, simplified tri-layer blue PhOLEDs were used to examine the GTZO and ITO anodes. The GTZO-based blue (green and red) PhOLEDs exhibited EL efficiencies of 19.0 %, (14.5% and 9.1%); while the control blue (green and red) PhOLEDs with the ITO anode exhibited efficiencies of 18.4 % (13.5% and 7.4%). These results show clear advantages for the use of GTZO as OLED anodes in terms of higher efficiency, electricity and luminance. The superior characteristics of this tailor-made GTZO film points toward the future replacement of ITO anode in future OLED applications.

The authors would like to thank the National Central University Optical Sciences Center for its technical support and Nano Science and Technology Center for providing research facilities. This work was financially supported by the National Science Council of Taiwan under Contract NSC 101-2221-E-155-034, NSC 102-2221-E-155-083, NSC 102-2221-E-155-080 -MY3, and

NSC 103-2623-E-155-008-ET.

References

1 K. Maejima, H. Shibata, H. Tampo, K. Matsubara and S. Niki, *Thin Solid Films*, 2010, **518**, 2949.

2 H.-K. Park, J.-W. Kang, S.-In. Na, D.-Y. Kim and H.-K. Kim, *Sol. Energy Mater. Sol. Cells*, 2009, **93**, 1994.

3 D. R. Sahu, S.-Y. Lin and J.-L. Huang, *Appl. Surf. Sci.*, 2007, **253**, 4886.

4 S. Y. Kuo, K. C. Liu, F. I. Lai, J. F. Yang, W. C. Chen, M. Y. Hsieh, H. I. Lin and W. T. Lin, *Microelectron. Reliab.*, 2010, **50**, 730.

5 W.-S. Liu, W.-K. Chen and K.-P. Hsueh, *J. Alloys Compd.*, 2013, **552**, 255.

6 J. Kang, H.-W. Kim and C. Lee, *J. Korean Phys. Soc.*, 2010, **56**, 576.

7 W.-S. Liu**,** W.-K. Chen, S.-Y. Wu and K.-P. Hsueh, *J. Am. Ceram. Soc.*, 2014, **97**, 473.

8 Z.-Z. Li, Z.-Z. Chen, W. Huang, S.-H. Chang and X.-M. Ma, *Appl. Surf. Sci.*, 2011, **257**, 8486.

9 H. J. Ko, Y. F. Chen, S. K. Hong, H. Wenisch, T. Yao and D. C. Look, *Appl. Phys. Lett.*, 2000, **77**, 3761.

10 V. Khranovskyy, U. Grossner, V. Lazorenko, G. Lashkarev, B. G. Svensson and R. Yakimova, *Superlattices Microstruct.*, 2006, **39**, 275.

11 J. J. Berry, D. S. Ginley and P. E. Burrows, *Appl. Phys. Lett.*, 2008, **92**, 193304.

12 J. Meyer, P. Görrn, S. Hamwi, H.-H. Johannes and T. Riedl, *Appl. Phys. Lett.*, 2008, **93**,

073308.

13 S. C. Gong, Y.-J. Choi, H. Kim, C.-S. Park and H.-H. Park, *J. Vac. Sci. Technol. A*, 2013, **31**, 01A101.

14 J.-W. Lim, S. J. Kang, S. Lee and J.-J. Kim, *J. Appl. Phys.*, 2012, **112**, 023513.

15 H. Chen, J. Ding and S. Ma, *Superlattices Microstruct.*, 2011, **49**, 176.

16 M. Jiang, X. Liu, G. Chen, J. Cheng and X. Zhou, *J. Mater. Sci.-Mater. Electron.*, 2009, **20**, 1225.

17 L. Xu, X. Li, Y. Chen and F. Xu, *Appl. Surf. Sci.*, 2011, **257**, 4031.

18 C.-Y. Tsay, H.-C. Cheng, C.-Y. Chen, K.-J. Yang and C.-K. Lin, *Thin Solid Films*, 2009, **518**, 1603.

19 T. Yamada, A. Miyake, H. Makino, N.Yamamoto and T. Yamamoto, *Thin Solid Films*, 2009, **517**, 3134.

20 H. Makino, Y. Sato, N. Yamamoto and T. Yamamoto, *Thin Solid Films*, 2011, **520**, 1407.

21 J.-M. Kim, P. Thiyagarajan and S-W. Rhee, *Thin Solid Films*, 2010, **518**, 5860.

22 M. Ohyama, H. Kozuka and T. Yoko, *J. Am. Ceram. Soc.*, 1998, **81**, 1622.

23 J. K. Sheu, K. W. Shu, M. L. Lee, C. J. Tun and G. C. Chi, *J. Electrochem. Soc.*, 2007, **154**, 521.

24 M. Kang, I. Kim, M. Chu and S. W. Kim, *J. Korean Phys. Soc.*, 2011, **59**, 3280.

25 S. Song, T. Yang, J. Liu, Y. Xin, Y. Li and S. Han, *Appl. Surf. Sci.*, 2011, **257**, 7061.

26 N. Serpone, D. Lawless and R. Khairutdinov, *J. Phys. Chem.*, 1995, **99**, 16646.

27 E. Burstein, *Phys. Rev.*, 1954, **93**, 632.

28 T.-S. Moss, *Proc. Phys. Soc. London Ser. B*, 1954, **67**, 775.

29 R. J. Holmes, S. R. Forrest, Y.-J. Tung, R. C. Kwong, J. J. Brown, S. Garon and M. E. Thompson, *Appl. Phys. Lett.*, 2003, **82**, 2422.

30 C.-H. Chang, Z.-J. Wu, Y.-H. Liang, Y.-S. Chang, C.-H. Chiu, C.-W. Tai and H.-H. Chang, *Thin Solid Films*, 2013, **548**, 389.

31 Y. Zheng, S.-H. Eom, N. Chopra, J. Lee, F. So and J. Xue, *Appl. Phys. Lett.*, 2008, **92**, 223301.

32 M. Mauro, C.-H. Yang, C.-Y. Shin, M. Panigati, C.-H. Chang, G. D'Alfonso and L. D. Cola, *Advanced Materials,* 2012, **24**, 2054.

33 S.-J. Su, T. Chiba, T. Takeda and J. Kido, *Adv. Mater.*, 2008, **20**, 2125.

34 C.-H. Chang, C.-L. Ho, Y.-S. Chang, I-C. Lien, C.-H. Lin, Y.-W. Yang, J.-L. Liao and Y. Chi, *J. Mater. Chem. C*, 2013, **1**, 2639.

35 S.-J. Su, E. Gonmori, H. Sasabe and J. Kido, *Adv. Mater.*, 2008, **20**, 4189.

36 D. Curiel, M. Más-Montoya, C.-H. Chang, P.-Y. Chen, C.-W. Tai and A. Tarraga, *J. Mater. Chem. C*, 2013, **1**, 3421.

37 H. Kim, J. S. Horwitz, W. H. Kim, S. B. Qadri and Z. H. Kafafi, *Appl. Phys. Lett.*, 2003, **83**, 3809.

38 Y. Tomita, C. May, M. Toerker, J. Amelung, M. Eritt, F. Loeffler, C. Luber, K. Leo, K. Walzer, K. Fehse and Q. Huang, *Appl. Phys. Lett.*, 2007, **91**, 063510.

39 J. H. Bae and H. K. Kim, *Thin Solid Films*, 2008, **516**, 7866.

40 J. W. Kang, W. I. Jeong, J. J. Kim, H. K. Kim, D. G. Kim and G. H. Lee, *Electrochem. Solid-State Lett.*, 2007, **10**, J75.

41 L. Wang, J. S. Swensen, E. Polikarpov, D. W. Matson, C. C. Bonham, W. Bennett, D. J. Gaspar and A. B. Padmaperuma, *Org. Electron*., 2010, **11**, 1555.

42 H. Lee, I. Park, J. Kwak, D. Y. Yoon and C. Lee, *Appl. Phys. Lett.*, 2010, **96**, 153306.

43 Z. L. Tseng, P. C. Kao, C. S. Yang, Y. D. Juang, Y. M. Kuo and S. Y. Chua, *J. Electrochem. Soc.*, 2011, **158**, J133.

Figure Captions:

Fig. 1 (a) XRD patterns of GTZO films deposited at various annealing temperatures. (b) Full width at half maximum (FWHM) and the (0 0 2) peak position of GTZO films deposited at various annealing temperatures.

Fig. 2 Optical transmittance of GTZO and ITO thin films prepared under various annealing temperatures. The magnified transmittance band edge between 320 and 400 nm for GTZO and ITO thin films were shown as the inset.

Fig. 3 Optical band gap of GTZO films prepared under various annealing temperatures. The optical band gap (E_g) is deduced by extrapolating the linear portion of a plot $(\alpha h\nu)^2$ against the ($h\nu$) axis. Inset summaries the optical band gaps of GTZO films with various annealing temperatures.

Fig. 4 Hall electrical resistivity (ρ), mobility (μ), and carrier concentration (n) of the GTZO films as a function of annealing temperature.

Fig. 5 Schematic structures of the tested OLEDs and structural drawing of the materials.

Fig. 6 (a) EL spectra of Devices B1, B2, G1, G2, R1, and R2 at a luminance of 10^3 cd/m^2, (b) current density-voltage-luminance (*J-V*) characteristics, (c) luminance-voltage (*L-V*) characteristics, (d) external quantum efficiency *vs*. luminance for the Devices B1, B2, G1, G2, R1, and R2.

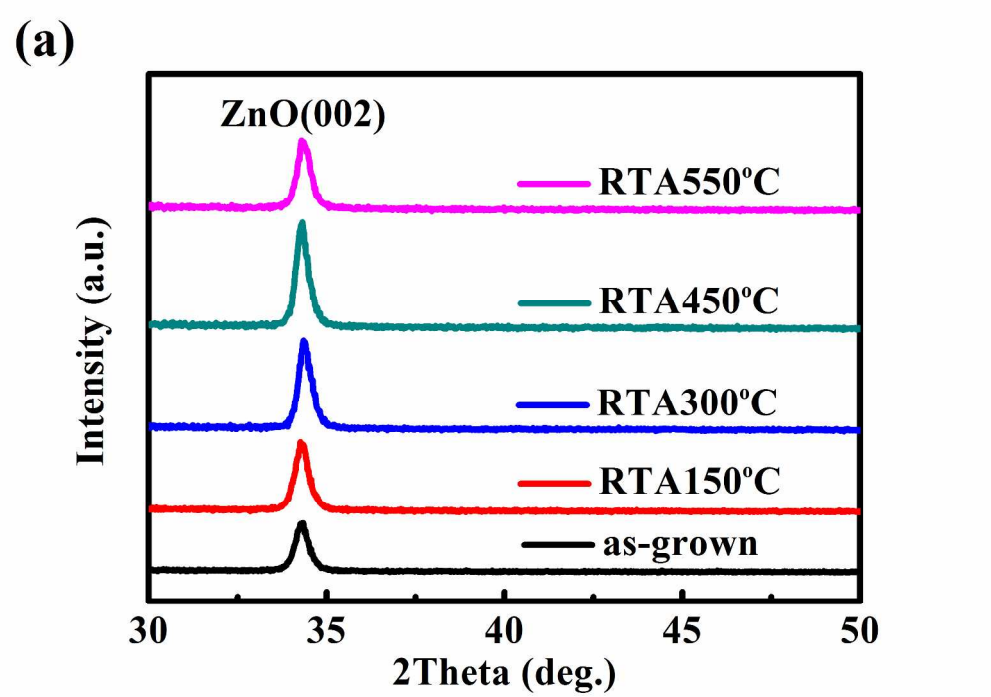

296x209mm (300 x 300 DPI)

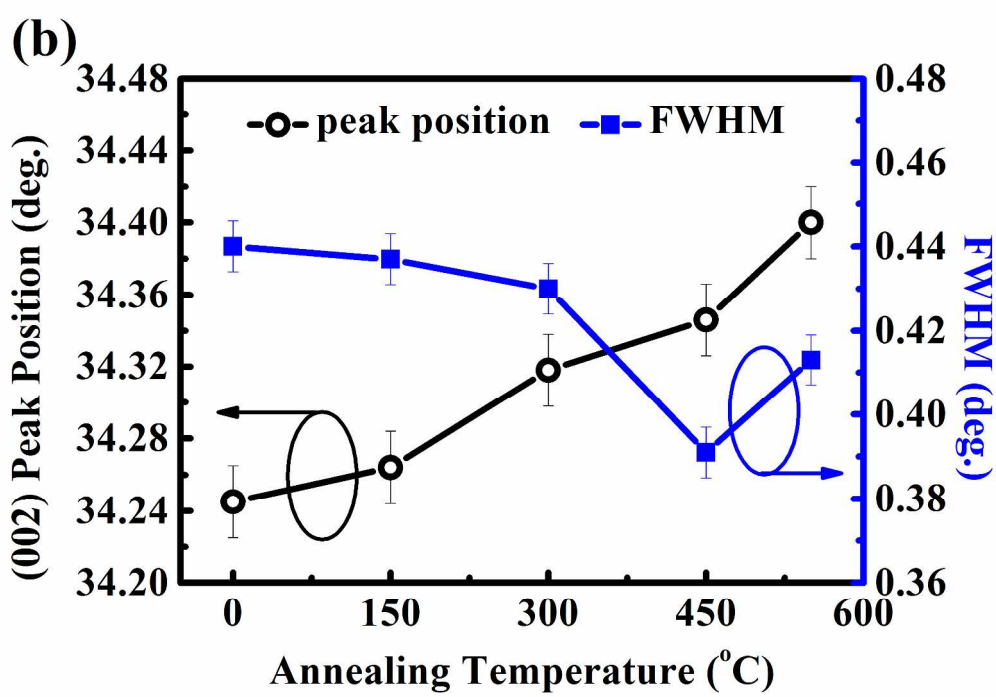

287x201mm (300 x 300 DPI)

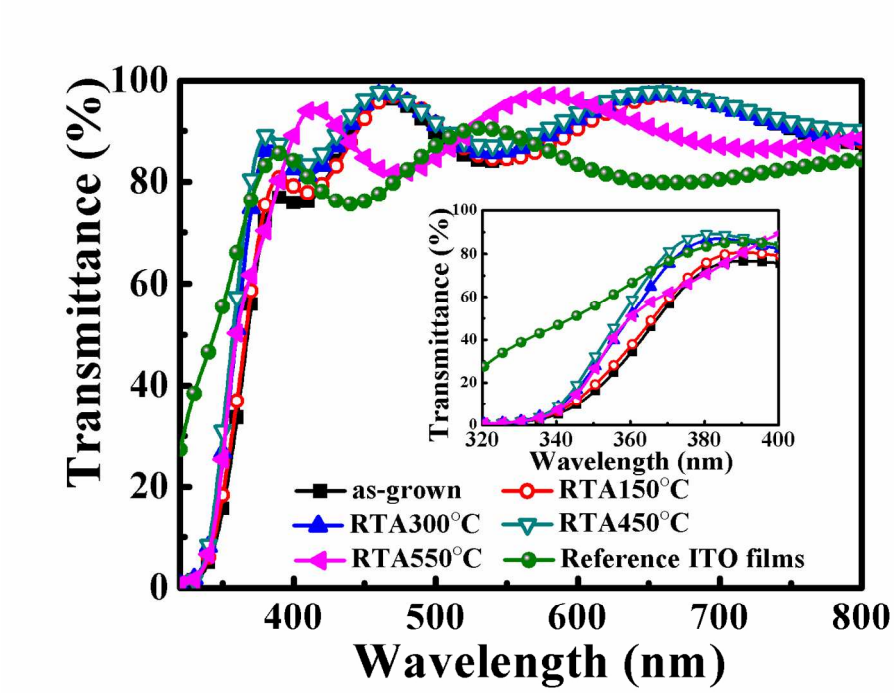

148x105mm (300 x 300 DPI)

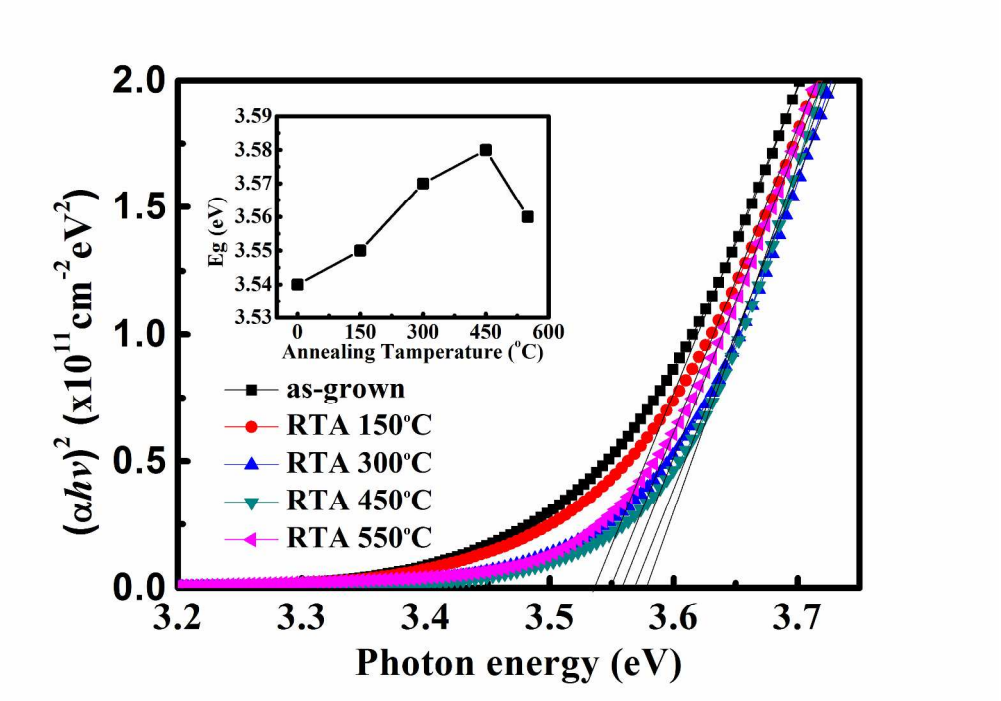

296x209mm (300 x 300 DPI)

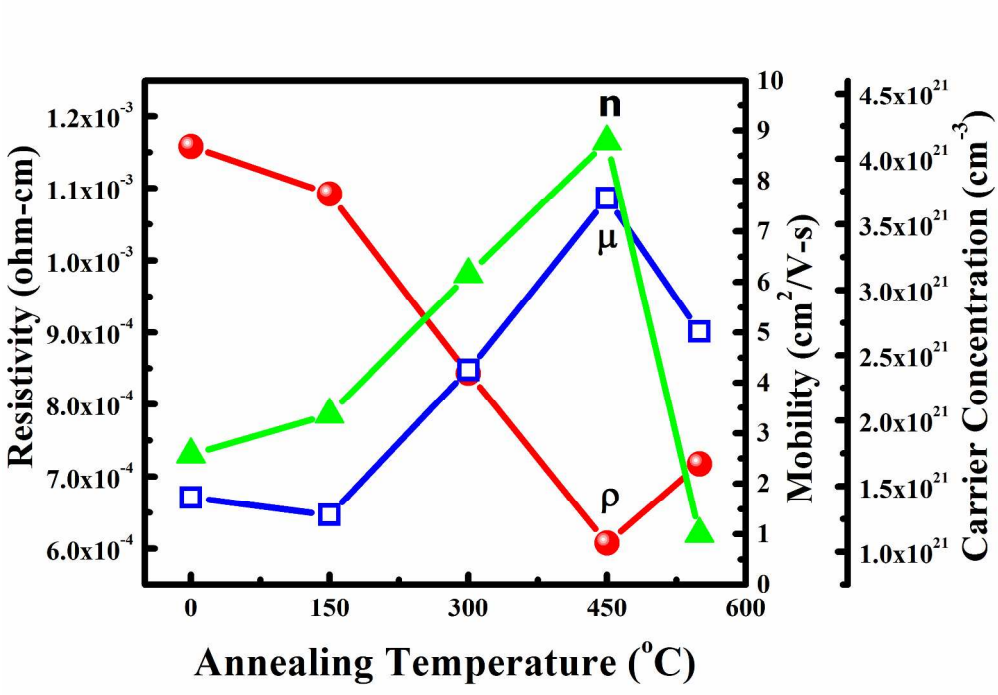

287x201mm (300 x 300 DPI)

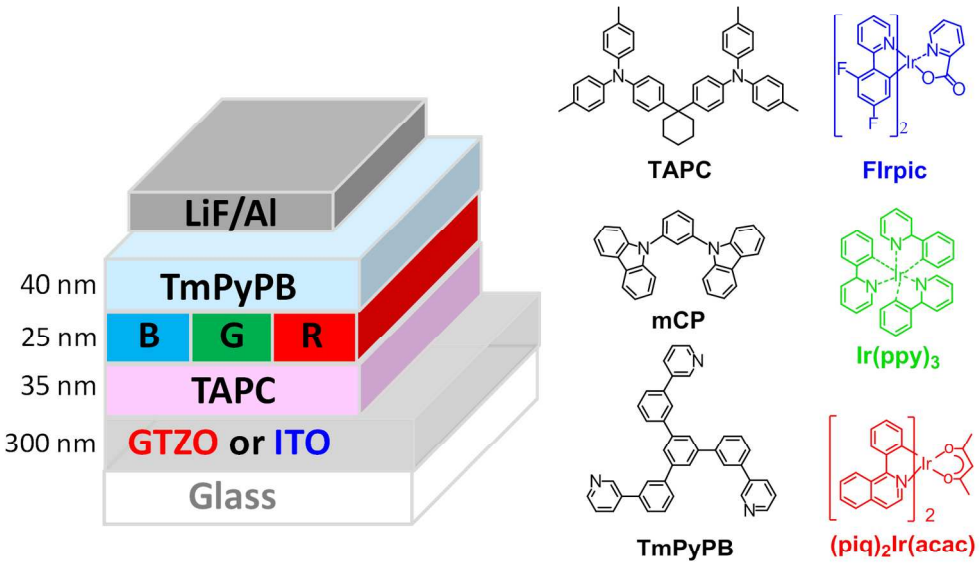

254x190mm (300 x 300 DPI)

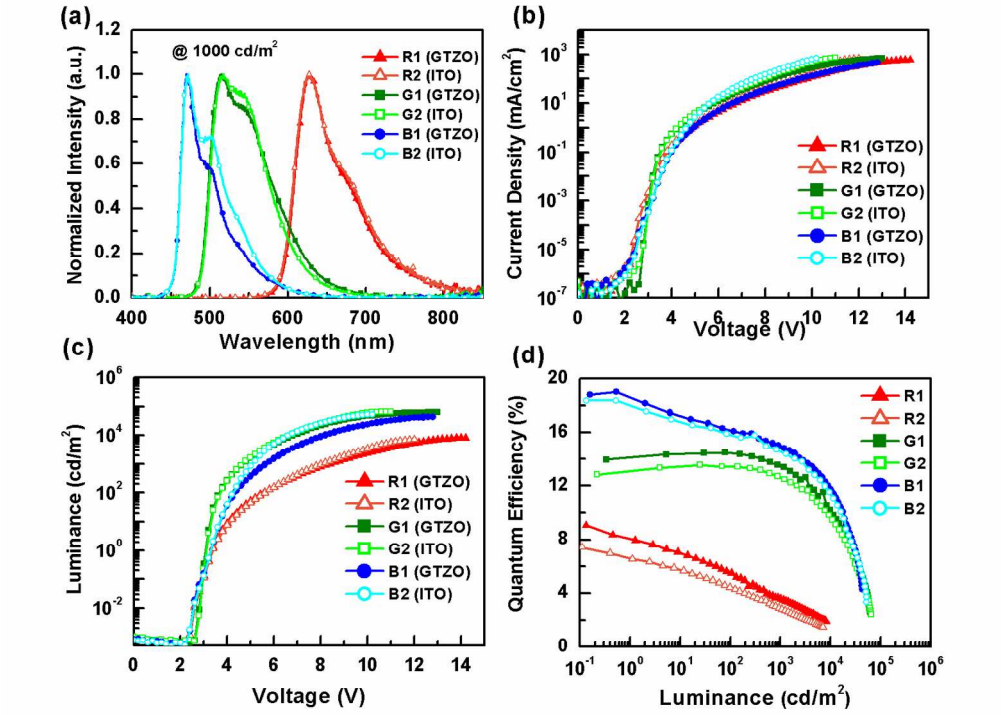

148x113mm (300 x 300 DPI)

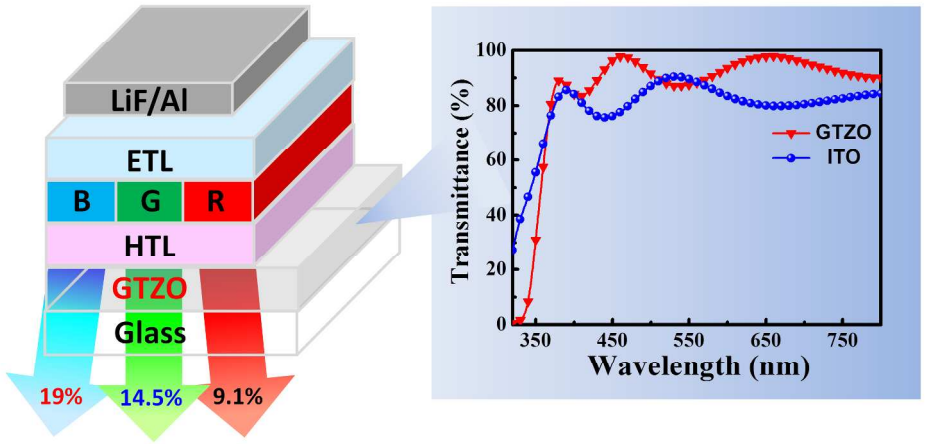

GTZO-based R, G, B PhOLEDs
254x190mm (300 x 300 DPI)